CRYSTAL GROWTH & DESIGN

Article

pubs.acs.org/crystal

Two Sets of Metal Organic Frameworks along the Lanthanide Series Constructed by 2,3-Dimethylsuccinate: Structures, Topologies, and Strong Emission without Ligand Sensitization

Germán E. Gomez,[†] María C. Bernini,[†] Elena V. Brusau,[†] Griselda E. Narda,*[,†] Walter A. Massad,[‡] and Ana Labrador[§]

[†]Area de Química General e Inorgánica "Dr. G. F. Puelles", Facultad de Química, Bioquímica y Farmacia, Chacabuco y Pedernera, Universidad Nacional de San Luis, Instituto de Investigaciones en Tecnología Química (INTEQUI-CONICET), 5700, San Luis, Argentina

[‡]Departamento de Química, Universidad Nacional de Río Cuarto, Campus Universitario, Río Cuarto, Argentina

[§]MAX IV Laboratory, Lund University, 221 00, Lund, Sweden

Supporting Information

ABSTRACT: Reactions in aqueous solution under hydrothermal conditions between (±)-2,3-dimethylsuccinic acid and lanthanide chlorides lead to two different isostructural types with chemical formulas $[Ln_2(C_6H_8O_4)_3(H_2O)_2]$ Ln(III) = Pr−Eu (except Pm) (Type I, compounds **1**−**4**) and $[Ln_2(C_6H_8O_4)_3]$ Ln(III) = Tb−Yb (except Tm) (Type II, compounds **5**−**9**). The crystal structure has been solved for the Pr (**1**)-, Sm (**3**)-, and Ho (**7**)-containing compounds by means of single-crystal XRD methods, whereas powder XRD Rietveld refinement was used for the rest of the MOFs. Compounds **1**−**4** crystallize in the triclinic space group $P\bar{1}$, whereas compounds **5**−**9** belong to the tetragonal space group $P4_32_12$. Type I and II compounds are 3D frameworks consisting of chains of $[LnO_8(H_2O)]$ or $[LnO_8]$ polyhedra, respectively, linked by dimethylsuccinate anions, giving rise to I^1O^2 connectivity. All the compounds were characterized by X-ray diffraction, variable-temperature Fourier transform infrared spectroscopy, and thermal analysis. An exhaustive topological study was performed in comparison with other related compounds. The photoluminescent (PL) properties for compounds **3**, **4**, and **5** have been also explored, indicating that a metal-centered luminescent process takes place.

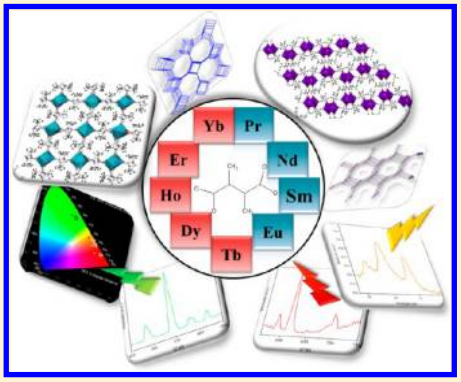

1. INTRODUCTION

Metal organic frameworks (MOFs)[1] have received intense interest mostly motivated by their intriguing variety of architectures and potential applications, mainly in relation to gas storage,[2] separations,[3] drug delivery,[4] etc. Since the beginning, most of the works have so far been focused on transition metals (TMs), though the use of lanthanides or rare earth ions (REE) has evidenced an important increase due to their diverse coordination numbers and interesting catalytic[5] and luminescent[6] properties, giving rise to attractive materials with fascinating motifs.

Regarding the linkers, aliphatic multicarboxylate ligands are considered as appropriate building blocks because of their flexibility along with their versatile coordination ability that offer various possibilities for constructing frameworks with unique structures and useful properties.[7]

The succinate ligand is a flexible dicarboxylate widely applied not only in the synthesis of TM ions-based frameworks[8] but also in those with REE ones, which allows the development of a great number of structures and topologies.[9] Moreover, REE succinate MOFs have been recently reported as heterogeneous catalysts[10] for the reduction of nitroaromatic compounds.

On the matter, we have previously synthesized and characterized several REE succinate frameworks with magnetic[11] and catalytic properties.[12] Besides, the use of the noncentrosymmetric 2,2-dimethyl-substituted succinate ligand (2,2-dms) has also been explored by us, thus obtaining two different laminar Er(III)-MOFs whose formation was governed by kinetic or thermodynamic control.[13] One of these compounds resulted in a pseudocentrosymmetric structure with the formula $[Er_2(2,2\text{-dms})_3(H_2O)_2]$, while the other one was centrosymmetric with the formula $[Er_2(2,2\text{-dms})_3(H_2O)]$, allowing us to study the influence of the *gem*-dimethyl substitution on the symmetry and architecture of the resultant frameworks.

Recently, several compounds employing yttrium or REE and 2,2-dms or 2,3-dimethylsuccinate (2,3-dms) have been reported by Cheetham and colleagues.[14] The frameworks containing the 2,2-dms linker exhibit 1D, 2D, and 3D connectivity overall, whereas those based on the 2,3-dms ligand are three-

Received: July 4, 2013
Revised: October 23, 2013
Published: October 25, 2013

   dx.doi.org/10.1021/cg401006d | *Cryst. Growth Des.* 2013, 13, 5249−5260

Table 1. Crystallographic Data for 1, 3, and 7

	1	3	7
crystal system	triclinic	triclinic	tetragonal
empirical formula	$Pr_2C_{18}H_{28}O_{14}$	$Sm_2C_{18}H_{28}O_{14}$	$Ho_2C_{18}H_{16}O_{12}$
formula mass	749.81	768.72	754.17
space group	$P\bar{1}$	$P\bar{1}$	$P4_32_12$
a [Å]	8.3626(12)	8.222(16)	17.764(3)
b [Å]	12.3940(18)	12.342(3)	17.764(3)
c [Å]	12.8469(18)	12.768(3)	15.355(3)
α [deg]	61.5989(2)	117.50(3)	90
β [deg]	86.515(2)	93.64(3)	90
γ [deg]	89.950(2)	90.02(3)	90
V [Å^3]	1168.5(3)	1146.29(5)	4845.3(14)
ρ_{calcd} [g·cm^{-3}]	2.121	2.200	2.068
Z	2	2	8
$F(000)$	724	738	2832
abs coeff [mm^{-1}]	4.189	5.143	6.539
crystal size [mm]	0.2 × 0.08 × 0.04	0.08 × 0.02 × 0.02	0.12 × 0.08 × 0.04
T_{min}/T_{max}	1.88/25.03	2.48/28.28	3.52/69.99
index ranges			
h	(−9,9)	(−10,0)	(−20,20)
k	(−14,14)	(−16,16)	(−21,17)
l	(−15,14)	(−16,17)	(−18,12)
reflns collected/unique with $I > 2\sigma(I)$	3982/3276	5203/4569	4409/3827
abs corr	semiempirical	semiempirical	semiempirical
refined parameters	313	325	313
goodness-of-fit on F^2	1.177	1.063	1.131
refinement method	full-matrix	full-matrix	full-matrix
	least-squares on F^2	least-squares on F^2	least-squares on F^2
final R indices	R_1 = 0.0632	0.0853	0.0587
[$I > 2\sigma(I)$]	wR_2 = 0.1518	0.2485	0.1316
R-factor-all	0.0830	0.0902	0.0681

dimensionally covalently bonded. The luminescent properties of some of these 1-D and 2-D nets doped with Eu and Tb have also been evaluated.

With the aim to extend our studies on REE succinate-based MOFs, the use of *meso*- or a racemic mixture of (±)-2,3-dms ligands has been investigated to explore the incidence of the conformational flexibility of the aliphatic subunits along with the coordination geometry preferences on the framework development. Here, we report the synthesis and crystal structure determination by single-crystal or powder X-ray diffraction with further refinement, and characterization by thermal analysis and variable-temperature Fourier transform infrared spectroscopy (VT-FTIR) of 9 compounds based on 2,3-dms and Ln(III), belonging to two different structural types: Type I, $[Ln_2(C_6H_8O_4)_3(H_2O)_2]$ with Ln(III) = Pr−Eu (except Pm), and Type II, $[Ln_2(C_6H_8O_4)_3]$ with Tb−Yb (except Tm). The emission spectra and the lifetime values of the Sm, Eu, and Tb compounds are also presented and analyzed in relation to their different structural features. Furthermore, the incidence of the water molecules in the photoluminescence (PL) performance of the Eu(III) compound is investigated. A topological revision including other related structures based on Ln(III) and succinate, 2,2-dms or 2,3-dms as linkers has also been performed.

2. EXPERIMENTAL SECTION

2.1. Synthesis. All the compounds were prepared under identical hydrothermal synthesis conditions, by dissolving 2,3-dimethylsuccinic acid (1.5 mmol) and the lanthanide chlorides (1 mmol) in 20 mL of distilled water. The pH value was adjusted to 3−4.5 with 0.1 mL of pyridine. The resultant mixtures were heated at 180 °C in a 120 mL Teflon-lined Parr bomb during 3 days; then, the reactor was immediately cooled to room temperature and the crystalline powders were washed with distilled water, filtered, and dried at room temperature. The obtained yields (%) based on the corresponding metal ions were 21.7 (**1**), 36 (**2**), 33.5 (**3**), 38.7 (**4**), 31.3 (**5**), 47.5 (**6**), 42.8 (**7**), 36.5 (**8**) and 45.9 (**9**). Crystals suitable for single-crystal X-ray diffraction analysis could be isolated for Pr (**1**), Sm (**3**), and Ho (**7**).

Purity of the samples was confirmed by comparison of the experimental and simulated XRD patterns. Detailed information about the synthetic procedure is available in the Supporting Information.

2.2. Single-Crystal Structure Determination. A single crystal of compound **1** was mounted on a Bruker-Siemens Smart CCD diffractometer equipped with a normal focus and a 2.4 kW sealed tube X-ray source (temperature = 296(2) K, Mo Kα radiation, λ = 0.71073 Å) operating at 40 kV and 30 mA.

Data were collected over a hemisphere of reciprocal space by a combination of three sets of exposures. Each set had a different θ angle for the crystal, and each exposure of 10 s covered 0.3° in ω. The crystal-to-detector distance was 5.5 cm. Unit cell dimensions were determined by a least-squares fit of reflections with $I > 2\sigma(I)$.

For compound **3**, X-ray diffraction data on a single crystal of dimensions 0.08 × 0.02 × 0.02 mm^3 were collected at the ESRF synchrotron in the Spanish BM16 beamline (Grenoble, France) using λ = 0.7378 Å at 100 K. The oscillation of the sample was performed with a single axis Huber 410 diffractometer equipped with an ADSC Q210r CCD detector. A complete description of the beamline is reported elsewhere.[15] Data were indexed, integrated, and scaled using the HKL2000 program.[16]

dx.doi.org/10.1021/cg401006d | Cryst. Growth Des. 2013, 13, 5249−5260

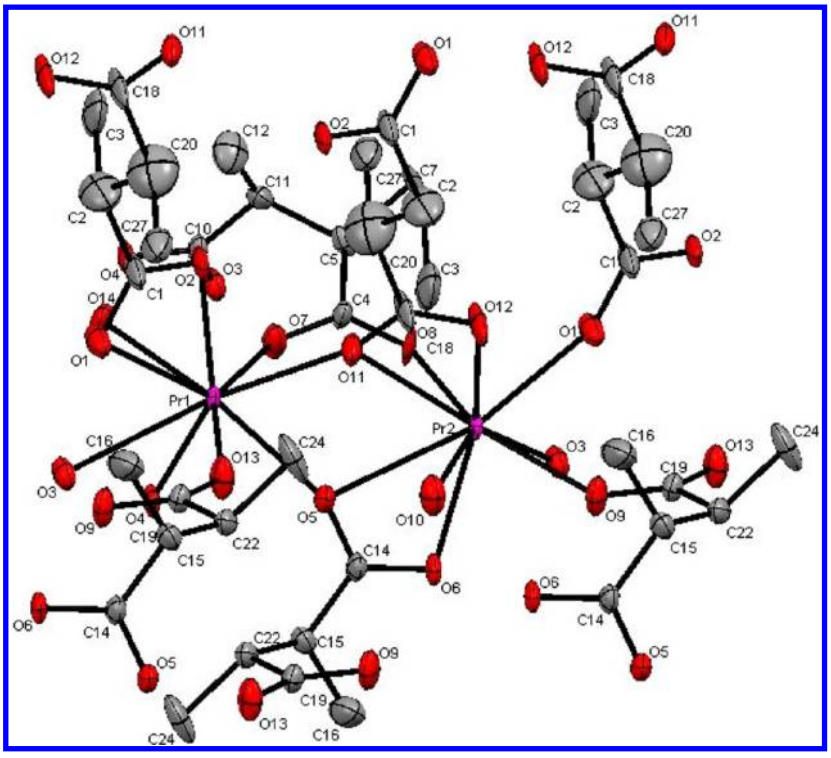

Figure 1. ORTEP drawing of the asymmetric unit of $[Pr_2(C_6H_8O_4)_3(H_2O)_2]$ (**1**); hydrogen atoms are omitted for clarity.

A single crystal of compound **7** was mounted on a Bruker four-circle kappa-diffractometer equipped with a Cu INCOATEC microsource operated at 30 W power (45 kV, 0.60 mA) to generate Cu Kα radiation (λ = 1.54178 Å) and a Bruker AXIOM area detector (microgap technology). Diffraction data were collected over a hemisphere of reciprocal space in a combination of φ and ω scans to reach a resolution of 0.8 A° (58.91° in θ), using a Bruker APEX2 software suite (each exposure of 10 s covered 0.5° in θ). Unit cell dimensions were determined by a least-squares fit of reflections with $I > 2\sigma(I)$.

A semiempirical absorption and scale correction based on equivalent reflection was carried out using SADABS[17] in all the structural determinations.

Space group determinations were carried out using XPREP.[18] The structures were solved by direct methods and refined by anisotropic full-matrix least-squares, except for hydrogen atoms of the ligand. A summary of conditions for data collection and structure refinement is given in Table 1. All calculations were performed using SMART software for data collection; SAINT plus program[17] for integration and scale correction of data; SHELXTL[18] to resolve and refine the structure and to prepare material for publication; and ATOMS[19] and MERCURY 2.0[20] for molecular graphics. Crystallographic information files (CIFs) corresponding to compounds **1**, **3**, and **7** have been deposited to the Cambridge Crystallographic Data Centre (CCDC numbers 947486−947488, respectively) and are also available in the Supporting Information of this work.

2.3. Powder X-ray Diffraction (PXRD). X-ray powder diagrams were obtained with a Rigaku D-MAX-IIIC diffractometer using Cu Kα radiation (λ = 1.5418 Å) and NaCl and quartz as external calibration standards. The best counting statistics were achieved using a scanning step of 0.02° between 5° and 60° Bragg angles with an exposure time of 5 s per step. The cell parameters of the compounds obtained as microcrystalline powders were refined applying the Rietveld method[21] procedures were performed using the FullProf[22] program.

2.4. Infrared Spectroscopy. FTIR spectra were recorded with a Nicolet Protégé 460 spectrometer in the 4000−225 cm^{-1} range with 64 scans, using the KBr pellet technique; spectral resolution was 4 cm^{-1}.

2.5. Thermal Analysis. Thermogravimetric analysis (TGA), differential thermal analysis (DTA), and differential scanning calorimetry (DSC) were performed with Shimadzu TGA-51, DTA-50, and DSC-60 apparatus under flowing air at 50 mL min^{-1} with a heating rate of 10 °C min^{-1}. X-ray powder diffraction was applied for further characterization of the pyrolysis products.

2.6. Solid-State Luminescence Measurements. Solid-state emission spectra were measured and lifetimes were determined on a Fluoromax 4P fluorescence spectrometer equipped with a photon counter having a photomultiplier R928P. Slit widths for excitation and emission were 3 nm. Luminescence spectra were recorded at room temperature between 450 and 750 nm under identical operating conditions without turning the lamp off to ensure a valid comparison between the emission spectra. The data were collected at every nanometer with an integration time of 100 ms for each step.

The luminescence decays were measured using the "decay by delay" feature of the phosphorescence mode with an integration time of 100 ms.

The excitation wavelengths for compounds **3**−**5** were 360, 397, and 257 nm and the emission ones 595, 615, and 543 nm, respectively. The repetition rates of the Xe flash lamp were 16 Hz (for **3**), 25 Hz (for **4**), and 20 Hz (for **5**) up to 300 flashes for **3**, 100 for **4**, and 50 in the case of **5** were accumulated per data point. The delays after flash were varied between 0.05 and 3 ms (for **3**), 0.05 and 1 ms (for **4**), or 0.05 and 10 ms (for **5**).

3. RESULTS AND DISCUSSION

3.1. Crystal Structures of Ln(III)-2,3-dms Compounds. The isostructural character of compounds **1**−**4** (Type I) was verified by comparison of the experimental PXRD patterns of the bulk materials with the simulated one from the single-crystal data obtained for compound **1** (see Figure S1, Supporting Information).

The same procedure was applied for compounds **5**−**9** employing the single-crystal XRD data of **7**, resulting in the second isostructural set (Type II) (see Figure S2, Supporting Information).

dx.doi.org/10.1021/cg401006d | Cryst. Growth Des. 2013, 13, 5249−5260

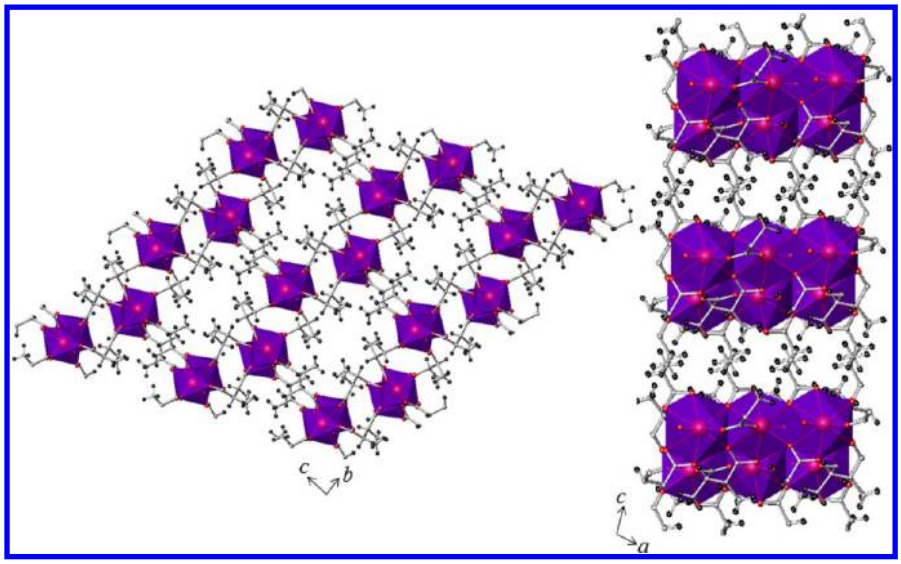

Figure 2. Structure of compound **1** showing the chains and their direction in the framework. The Pr atoms and polyhedra are burgundy and blue, respectively. The carbon, oxygen, and hydrogen atoms are in gray, red, and black, respectively.

Then, the structural refinement of the polycrystalline samples belonging to Type I and II compounds was performed by the Rietveld method, starting from the known models of the isostructural compounds **1** and **7**, respectively (see Figures S3 and S4 and Tables S1 and S2, Supporting Information).

*3.1.1. Type I Compounds (**1**–**4**).* The structural description is based on the single-crystal data of **1**, and specific information of **3** will be given when necessary. The compounds crystallize in the triclinic $P\bar{1}$ space group (S.G.); the cell parameters for compounds **1** and **3** are shown in Table 1, whereas the corresponding data for **2** and **4** are listed in Table S1 (Supporting Information). There are two crystallographically nonequivalent Ln(III) ions, both with a nine coordination number, and three independent 2,3-dms anions in the asymmetric unit. As an example, the coordination environment of the Pr-based compound is shown in Figure 1. Both Ln1 and Ln2 are surrounded by eight oxygen atoms coming from carboxylate groups and one oxygen atom from a coordinated water molecule. The coordination geometry of both metal centers is consistent with a monocapped square antiprism.

The Pr1–O bond lengths fall in the range 2.42(1)–2.724(9) Å, whereas the Pr2–O ones are in the range of 2.42(1)–2.725(8) Å. In the case of compound **3**, the corresponding distances are between 2.373(9) and 2.687(9) Å for the [Sm1–O_9] polyhedron and between 2.380(10) and 2.676(9) Å for the [Sm2–O_9] one.

The 2,3-dms anions adopt a *trans* conformation [torsion angle (C1–C2–C20–C18), 179(1)°], and two *gauche* conformations [torsion angles (C4–C5–C11–C10), −67(1)°, and (C19–C22–C15–C14), 68(1)°]. Each ligand links four metal ions; the *trans*-dms conformer coordinates as a chelate-bridge by its two carboxylate groups, whereas the *gauche* ones present the same coordination mode by one carboxylate extreme and a bidentate-bridge mode by the other one.

The SBU runs along the *a* direction and consists of chains of [$PrO_8(H_2O)$] edge-sharing coordination polyhedra (Figure 2). The chains are connected along the *b* direction by the *gauche*-dms ligands, whereas the *trans*-dms ones provide connection in the *c* direction.

One strong H-bond interaction was identified in the structure, involving one oxygen atom of a carboxylate group of one *gauche*-dms isomer and the coordinated water molecule, the O···H distance being equal to 1.79 Å.

According to both organic connectivity between metal centers and extended inorganic connectivity, these compounds can be classified as I^1O^2, where I^1 means that the inorganic connectivity is 1D and O^2 implies that the organic one is 2D, which involves organic "linkers" connecting the SBUs in two crystallographic directions; the sum of the exponents gives the overall dimensionality of the structure.[23]

The structure of Type I compounds is very similar to that of a La(III)-2,3 dms compound recently reported[14] also consisting of [$LnO_8(H_2O)$] chains linked by 2,3-dms anions with the same coordination modes, giving an analogous 3D structure. However, such a compound belongs to the monoclinic *C*2/*c* S.G. and presents the backbone of the *trans*-2,3-dms conformer strongly disordered over two sites.

Attempts to solve the structure of compounds **1** and **3** in such a monoclinic S.G. gave a worse result, with higher *R* values and goodness-of-fit on *F* (GOF) parameter. This fact indicates that the solution and refinement of the model in the *C*2/*c* S.G. does not seem to be the best choice, at least in our case. Presumably, single crystals of **1** and **3** have better crystalline quality (which is evident, for example, from the absence of disorder in the ligands), allowing us to solve and refine the structure in the triclinic system ($P\bar{1}$ S.G.). Moreover, when models of **1** and **3** were analyzed with the ADDSYM Exact application of the Platon Program[24] in order to rule out the existence of higher-order symmetry, no other S.G. was suggested.

The 2,3-dimethyl substitution on succinate appears not to affect substantially the ligand flexibility, since the *gauche* and *trans* conformers are present in a 4:2 ratio, respectively, in each coordination environment. The same ratio was also observed in three 3D Ho(III) succinate frameworks previously reported by us.[11,25] Specifically, the analysis of the crystal structure of the Type I compounds reveals their isomorphic character with the $[Ho_2(C_4H_4O_4)_3(H_2O)_2]\cdot 0.33(C_7H_6O_3)$ structure[25] (named **succ1** from now on) whose cell parameters are *a* = 7.611(2)

dx.doi.org/10.1021/cg401006d | *Cryst. Growth Des.* 2013, 13, 5249–5260

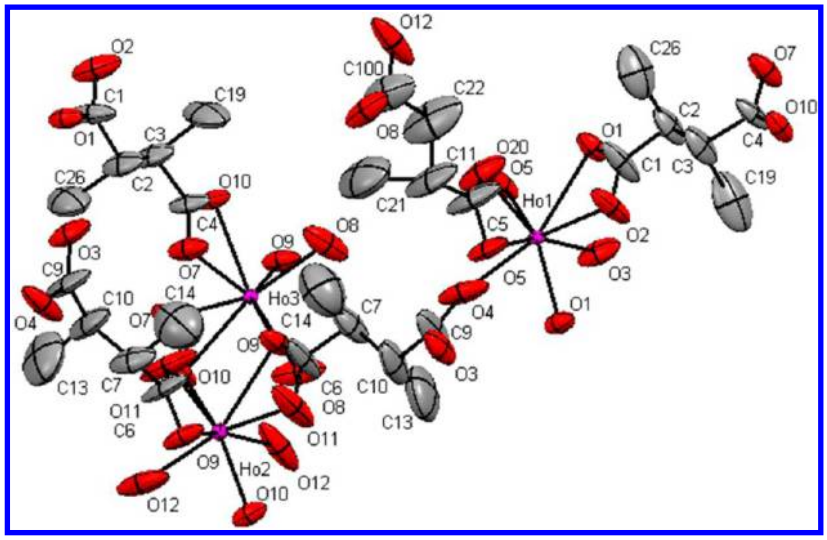

Figure 3. ORTEP drawing of the asymmetric unit of $[Ho_2(C_6H_8O_4)_3]$ (7); hydrogen atoms are omitted for clarity.

Å, b = 11.927(3) Å, c = 12.130(3) Å, α = 67.602(4)°, β = 89.920(4)°, γ = 80.498(4)°, and V = 1001.8(4) Å^3.

According to ref 14, it is quite noticeable that two-thirds of the 2,3-dms ligands in the La(III) framework analogue adopt a *gauche* conformation, which implies that both methyl substituents are oriented to the same side of the ligand involving a higher energy conformation in comparison to the *trans* one. However, the *gauche effect* is a known fact that justifies the preference of the *gauche* conformation in different 1,2-substituted ethanes.[26] In addition, it was demonstrated by DFT calculations in our previous work on 2,2-dms MOFs,[13] that *gauche* conformers can be thermodynamically more stable than the *trans* ones. Coordination attractive forces, strong H-bond interactions involving the *gauche* conformers, along with the presence of structure directing agents (SDAs), can drive the framework development, forcing the aliphatic backbone to adopt different conformations in order to achieve the whole framework stabilization.

*3.1.2. Type II Compounds (**5**–**9**).* The crystal structure of compound **7** as representative of these phases will be presented. It crystallizes in the tetragonal $P4_32_12$ S.G.; the asymmetric unit (Figure 3) contains three nonequivalent Ho(III) cations, two of them located on a special position corresponding to the 4*a* *Wyckoff site*, and also three dms ligands exhibiting a *quasi trans* conformation, with dihedral angles of ∼164° for two of them and 171° for the remaining one. One of these linkers is disordered over two sites with approximately half occupancy of each component present. An isostructural compound based on Y(III) and 2,3-dms has been recently reported[14] having all the ligands disordered over two positions; however, such a structure is enantiomorphic to that of **7** since it belongs to the $P4_12_12$ S.G. Such a difference could be related to different synthesis conditions (200 °C and KOH to regulate the pH instead of 180 °C and pyridine in our case). The influence of the different synthesis temperatures is also clear in the higher degree of positional disorder the dms linkers exhibit in the Y(III) analogue in relation to **7**.

The coordination environment around the Ho(III) ions involves eight oxygen atoms, all coming from carboxylate groups; the corresponding Ho1–O, Ho2–O, and Ho3–O distances are in the ranges of 2.228(9)–2.576(8), 2.223(10)–2.563(8), and 2.296(8)–2.520(8) Å, respectively. The high similarity in the ionic radii between octacoordinated Y(III) and Ho(III) ions (1.019 and 1.015 Å, respectively) is evident in the resultant Y–O distances, which lie in the ranges 2.207(8)–2.54(2), 2.257(11)–2.53(3), and 2.201(14)–2.56(2) Å, for Y1–O, Y2–O, and Y3–O, respectively.

The $[HoO_8]$ polyhedra are linked together in chains by sharing edges and run along the *c* direction; these 1D inorganic SBUs are further connected through the organic linkers developing an I^1O^2 3D structure (see Figure 4). The ligands

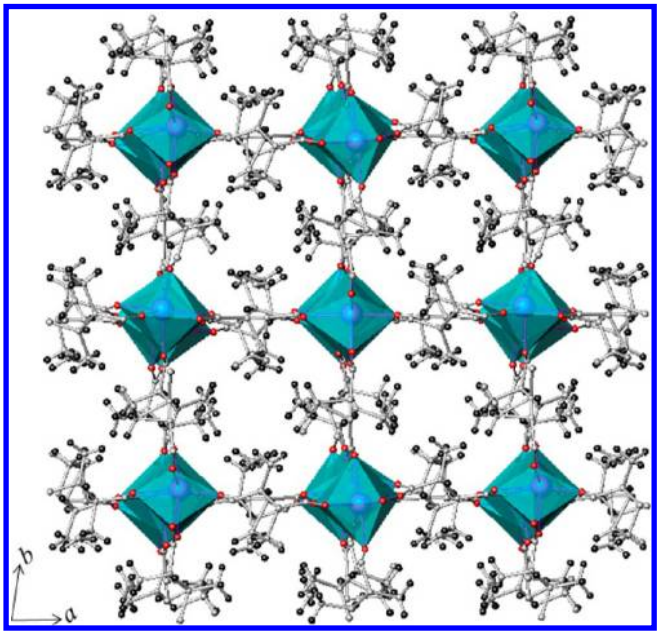

Figure 4. Structure of compound **7** along the *c* direction. The Ho atoms and polyhedra are blue and the carbon, oxygen, and hydrogen atoms are gray, red, and black, respectively.

exhibit the same coordination modes, that is, chelate-bridge by one carboxylate group and bidentate-bridge by the other one. The methyl groups are oriented toward the square channels with an available void volume of 182 Å^3, equivalent to 3.8% of the unit cell (calculated with Platon[24]).

3.2. Synthetic and Structural Trends in Ln(III)-2,3-dms and Related Frameworks. It is important to remark that

dx.doi.org/10.1021/cg401006d | *Cryst. Growth Des.* 2013, 13, 5249–5260

Table 2. Summary of the Topological Analysis

compound	formula	space group	point symbol	topology type	ref
1−4	$[Ln_2(2,3\text{-dms})_3(H_2O)_2]$	$P\bar{1}$	$4^6.6^4$	**bnn**	this work
La-2,3dms	$[La_2(2,3\text{-dms})_3(H_2O)_2]$	$C2/c$			14
succ1	$[Ho_2(succ)_3(H_2O)_2]\cdot n$Ar	$P\bar{1}$			25
5−9	$[Ln_2(2,3\text{-dms})_3]$	$P4_32_12$	$4^6.5.6^3$	**fni**	this work
Y-2,3dms	$[Y_2(2,3\text{-dms})_3]$	$P4_12_12$			14
Eu-2,2dms	$[Eu_2(2,2\text{-dms})_3(H_2O)_3]$	$Pccn$	$(4.6.8)(4.6^2)(4^2.6^3.8)(4^2.6^5.8^3)(4^2.6)$	novel type	14
Tb-2,2dms	$[Tb_2(2,2\text{-dms})_3(H_2O)_3]$				14
Lu-2,2dms	$[Lu_3(2,2\text{-dms})_4(OH)]$	$P2_1/c$	6^6	**dia**	14

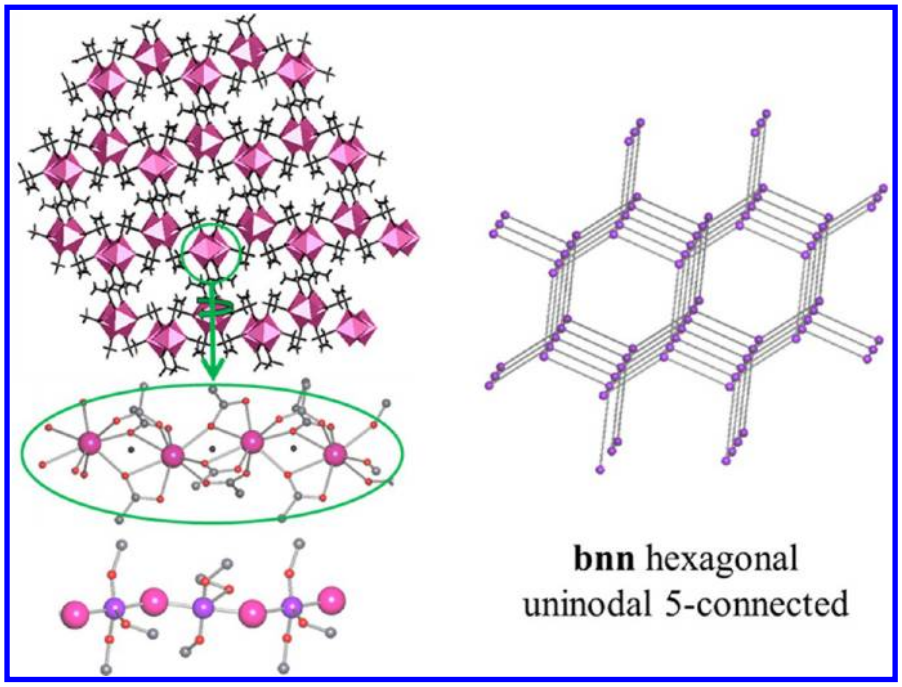

Figure 5. Topological description of compounds **1−4** based on the SBU packing.

compounds **1−9** were obtained under identical synthesis conditions, demonstrating that the structural differences found are mainly due to the incidence of the decrease of the ionic radii along the lanthanide series.

As it was already mentioned, the structural Type I was isomorphic with **succ1**.[25] A primary template effect of salicylic acid, benzene, and acetylsalicylic acid was verified in the formation of **succ1**-like phases, while a structure directing agent function (SDA) was determined when pyridine was added as an auxiliary molecule in the synthesis. In all the cases, large amounts of these aromatics were used in the synthesis and a direct correlation between the compound purity and the quantity of the aromatic agents was verified. About 60 mmol of pyridine per 0.75 mmol of succinate was needed to obtain the corresponding **succ1**-like structure ($[Ho_2(C_4H_4O_4)_3(H_2O)_2]\cdot 2H_2O$, named 1-Py in ref 25) in pure form, whereas only 0.62 mmol of pyridine per 0.75 mmol of 2,3-dms is required to obtain the isomorphic Type I compounds as pure phases. Thus, an SDA function of pyridine can be also proposed in the formation of these compounds with an alkyl-substituted succinate ligand. However, unlike the phase where two water molecules act as space-filling species, the lower requirement of pyridine can be justified considering the main channels are occupied by the bulky methyl groups that stabilize the voids without incorporating solvent molecules. As a result, the effective available void volume of the framework descends from 215 Å^3 (equivalent to 21.5% of the cell volume) to 48.6 Å^3 for **1** and 52.5 Å^3 for **3** (equivalent to 4.2% and 4.6% of the cell volumes, respectively).

Moving from the structural Type I to II, the most important differences are the diminution in the coordination number of the lanthanide ions (from 9 to 8) and the absence of coordinated water molecules in the second one. Despite both types present, the same covalent connectivity, a preference of the dms linkers to adopt only *trans* conformations, was verified in the Type II compounds. This fact is related to the steric requirements of a lower coordination number, since *trans* conformers are less voluminous than the *gauche* ones, being more easily accommodated in a restricted coordination environment.

Thus, the methyl substitution on the 2- and 3-positions of the succinate does not seem to affect the ligand flexibility, resulting in similar coordination ability as the nonsubstituted analogue linker, which is evidenced in the high tendency to develop 3D frameworks with I^1O^2 covalent connectivity, as it is demonstrated in these new sets of compounds and others previously reported.[14]

Besides, the 2,3-dimethyl substitution maintains a higher degree of symmetry in the ligand in comparison with the 2,2-dimethyl one, which is apparent from the number of noncentrosymmetric structures obtained with the *gem*-dimethyl-substituted succinate isomer.[13,27] This substitution

dx.doi.org/10.1021/cg401006d | *Cryst. Growth Des.* 2013, 13, 5249−5260

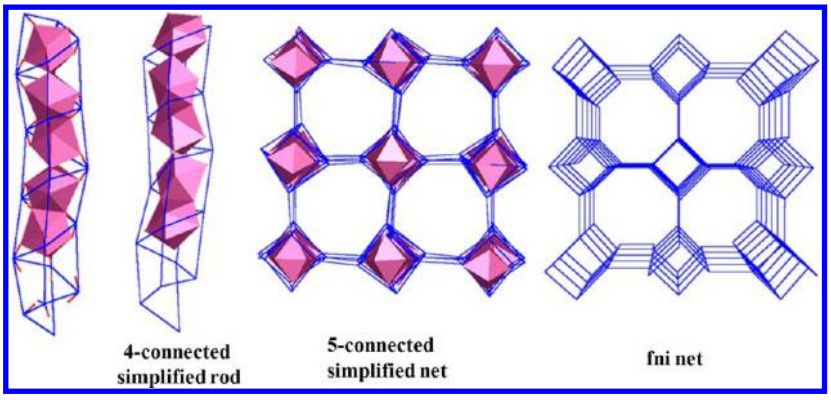

Figure 6. Topological description of compounds **5**–**9** based on the SBU packing.

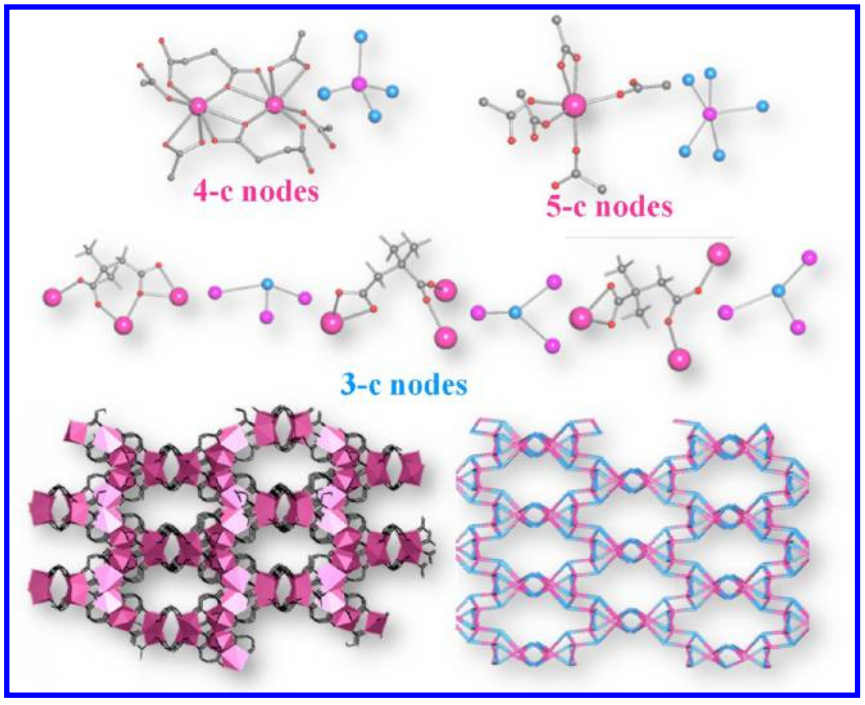

Figure 7. Topological description of compounds **4** and **5** from ref 14.

strongly influences the ligand flexibility and its coordination ability, leading to frameworks with minor dimensionality, mostly 2D.[14]

3.3. Topological Study. As it was already mentioned, several Ln (or Y)-MOFs based on alkyl-substituted succinate ligands have been recently reported.[13,14] Fourteen of them contain the *gem*-dimethylsuccinate as linker, whereas the remaining ones the 2,3-dms isomer. In such a large variety of compounds, only five of them exhibit a 3D covalent connectivity, reflecting the strong influence of the 2,2-dimethyl substitution toward conformations that favor the development of 2D frameworks. In this sense, obtaining the *underlying topology* allows one to extract the innate structure of the net associated with such a crystal structure.[28] From this perspective, different compounds based on related components are analyzed in a singular and more general way in order to understand the resultant structural global features. The connectivity of the building blocks is considered to find resemblances or differences among diverse frameworks. The obtained simplified nets are classified considering the ideal nets present in the Reticular Chemistry Structure Resource Database, and a three letter code symbol such as **abc** or a symbol with extensions such as **abc-d** is assigned.[29] Definitions and recommended terminology to characterize the simplified nets, can be found in ref 30. Thus, a topological revision including the 3D structures reported in ref 14 and the new 3D frameworks studied in this work has been performed. To this aim, the TOPOS[31] and Systre[32] programs were employed, and the corresponding results are displayed in Table 2.

It is worth mentioning that the 3D structures under analysis include both 0D and 1D inorganic SBUs. Besides, among those with 0D SBUs, some of them—the isostructural compounds based on Eu or Tb and 2,2-dms[14]—feature alternating rows of dimers of LnO_8 polyhedra and isolated pairs of LnO_8 polyhedra, whereas the compound based on Lu and 2,2-dms[14] exhibits trimeric clusters as inorganic building blocks. For this reason, different simplification procedures were applied to the frameworks according to the constitution of their SBUs.

The topology of the compounds belonging to Type I (**1**–**4**) can be described in terms of the rod-shaped SBU packing.[33] Thus, if a ghost atom is inserted at the centroid position between both metallic centers (see Figure 5), this atom

dx.doi.org/10.1021/cg401006d | *Cryst. Growth Des.* 2013, 13, 5249–5260

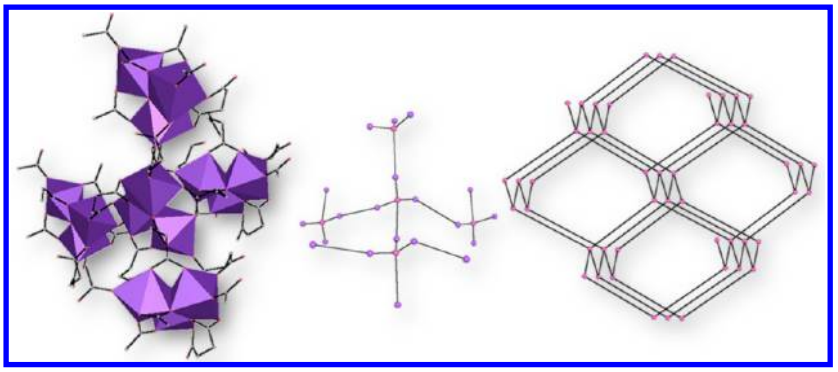

Figure 8. Topological description of compound **12** from ref 14.

acquires three connections to the nearest carboxylate groups and two additional bonds to the adjacent Ln(III) ions. As a result, the rod-shaped SBU is simplified and represented by 5-connected nodes and the resultant net is hexagonal **bnn** type (point symbol: $(4^6.6^4)$ and vertex symbol[30] (VS) [4.4.4.4.4.4.6.6.6.*]). The same topology was obtained for the isomorphic **succ1** compound,[25] and it is also associated with the structure of the La and 2,3-dms phase reported in ref 14.

The simplified net of the Type II compounds (**5**–**9**) was obtained using the Systre program. The carboxylate C atoms were used as the points of extension of the inorganic chains as the simpler way to deconstruct the net keeping the rod shape of the SBU. Regulating the distance considered from this point, a 4-connected rod was obtained, giving rise to a 5-connected uninodal net (see Figure 6). Such a description corresponds to the **fni** topological type (point symbol for the net $(4^6.5.6^3)$, VS:[30] $[4.4.4.4.4.4.5_3.9_7.9_7.*]$), which is a chiral tetragonal net consistent with the symmetry of the whole structure.

The MOFs based on Eu(III) (or Tb) and 2,2-dms[14] were topologically studied by means of the standard simplification procedure taking into account the number of metal centers that each 2,2-dms connects and the number of carboxylate groups belonging to different ligands in the Ln(III) coordination environment (see Figure 7). This methodology is the most suitable since the SBU is composed of alternating dimers and isolated polyhedra. The resultant simplified net contains three kinds of vertices: 3-connected (dms ligands), 4-connected (LnO_8 dimers), and 5-connected nodes (isolated LnO_8 polyhedra). The point symbol for the net is $(4.6.8)(4.6^2)$-$(4^2.6^3.8)(4^2.6^5.8^3)(4^2.6)$, and as far as we know, it would correspond to a novel topological type.

The compound containing Lu(III) and 2,2-dms[14] features SBUs composed of trimers of LuO_7 polyhedra, all bonded to a central hydroxide group. The most appropriate procedure to deconstruct its framework consists of the cluster simplification method by which the whole trimer is represented by the central μ_3-OH group; the connectivity of such a node is determined by counting the number of trimers bonded to the central one (see Figure 8). As can be seen, each trimer is connected to four other ones in a tetrahedral geometry, giving as a result a **dia** net.

It can be assessed from the topological analysis that, under high synthesis temperature and high metal content, the dms ligand tends to develop frameworks with condensed inorganic SBUs (finite, as in LuO_7 trimers, or infinite 1D chains as in the compounds of this work and compounds **13** and **14** from ref 14). These kinds of structures can be easily simplified considering the packing of such SBUs, giving underlying nets that are highly symmetric and generally uninodals, since the ligands are usually simplified as linker lines. On the contrary, at lower temperatures and metallic content in the synthesis, the inorganic polyhedra remain isolated in the structure, rendering more complicated topologies due to all topological roles (those of the metal centers and those of the ligands) are equally important. These kinds of nets frequently have more than one type of node, as it was observed in the underlying nets of Eu(III) (or Tb) and 2,2-dms MOF of ref 14 and that of the 2D Er(III)-succinate reported by us.[34]

3.4. Thermal Analysis. Table S3 in the Supporting Information summarizes the thermal data for all the compounds; Δm % values calculated on the basis of the determined stoichiometries—present in parentheses—show a good agreement with the experimental ones. The corresponding TGA and DTA curves are shown in Figures S5–S13 (Supporting Information).

For Type I compounds, the elimination of the coordinated water molecules is observed at slightly increasing temperatures as the ionic radii decrease according to the lanthanide contraction. The dehydration process is associated with a weak endothermic signal in the DTA curves that is hard to appreciate in the cases of **3** and **4** for which the corresponding DSC experiments were performed (see insets in Figures S7 and S8, Supporting Information). Although the MOFs retain their crystalline character upon dehydration, as it is usually expected from their 3D covalent structure, a decrease of crystallinity is evidenced, accounting for a partial structural disorder derived from the thermal treatment. The X-ray patterns corresponding to the dehydrated Type I compounds are gathered in Figures S14 and S15 (Supporting Information), from which it can be observed that dehydration leads to a structure different from those of compounds **1**–**4** and **5**–**9**. It is also noticeable that some lines disappear with water removal, this effect being more marked for compounds **3** and **4**. An analysis of the crystallographic data indicates that these reflections correspond to *hkl* planes that mainly involve the water molecule and those carboxylate groups that exhibit the chelate-bridging coordination mode. This fact suggests a rearrangement of the coordination environment around the Ln(III) inducing conformational modifications in all the dms conformers. Thermal evolution proceeds with the decomposition of the organic linkers through several steps, leading to the formation of the corresponding oxides. The corresponding mass decays are accompanied by strong exothermic DTA peaks.

The TGA and DTA curves of Type II compounds present a unique event denoted by an important weight loss and an exothermic peak, respectively. No evidence of phase transition was found.

dx.doi.org/10.1021/cg401006d | *Cryst. Growth Des.* 2013, 13, 5249–5260

The thermal stability of the frameworks increases gradually from **1** to **9**. The **succ1** compound and the related La(III)-MOF[14] fit this trend very well. It is worth mentioning that, under identical synthesis conditions, but using succinate as ligand, a compound with a different structure and lower thermal stability is obtained.[12]

3.5. Vibrational Study. The compounds belonging to each structural type exhibit identical vibrational behavior, and therefore, one compound of each structural type was selected. Figure 9 shows the FTIR spectra at room temperature of

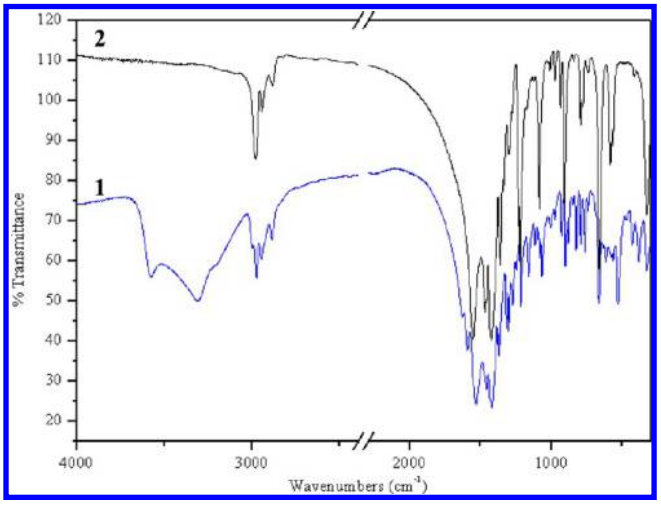

Figure 9. FTIR spectra of compounds **1** (1) and **7** (2).

compounds **1** and **7**. The interpretation of the IR spectra was performed by considering the most important internal vibrations of water molecules, carboxylates, and methyl groups and their comparison with those observed in H_2dms and other related compounds.[13,25] The IR frequency values for compound **7** are reported in parentheses.

3.5.1. Water Modes in Compound 1. The assignment of these modes, particularly the librational ones, was performed by comparing the spectra of partially and completely dehydrated samples obtained with a variable-temperature-IR (VT-FTIR) cell (Figure S16, Supporting Information). The corresponding thermal data were taken into account.

A broad band can be observed in the OH stretching zone in the IR spectrum. The band shows several components consistent with the presence of water molecules that are involved in coordination to the metal ion but also in hydrogen bonds in the lattice: 3579 (ν_{as}), 3309 and 3201 (ν_s) cm^{-1}. The band located at 1627 cm^{-1} is associated with the bending mode of the coordinated water molecules, whereas several librational modes (rocking, twisting, and wagging) are observed in the 1000−600 cm^{-1} range.

3.5.2. Carboxylate Groups Modes. Both carboxylate stretching modes are present in the FTIR spectra as asymmetric bands. The splitting of these modes can be explained in terms of the different types of interactions between the carboxylate groups and the Ln(III) cations found in the crystals of both compounds. The bands at 1591 and 1535 cm^{-1} (1550) are assigned to the ν_{as}(OCO), whereas a pair of bands at 1380 and 1369 cm^{-1} (1338 and 1302) are associated with the corresponding symmetric mode. No evidence of carbonyl absorption is present.

3.5.3. Methyl Groups Modes. The bands located at 1456 and 1419 cm^{-1} (1467) are assigned to $\delta_{as}(CH_3)$.

3.6. Luminescent Properties. Since the first investigation dealing with MOFs luminescence in 2002, about 200 articles and a few reviews reporting these properties have been published in the literature. Such a number is quite minor by far than the total number of publications regarding MOFs,[35] although several interesting results have been shown in relation to Ln(III)-based MOFs,[6,36] affording inspiration to continue investigation in fluorescence properties of these kinds of materials.

The lanthanide fluorescence is characterized by low absorbance coefficients and low quantum yields since the Ln electronic transitions are forbidden by parity (Laporte) selection rules,[36a] making the direct excitation of the metals very inefficient unless high-power laser excitation is utilized. However, the introduction of chromophores as linkers or guest species can help to overcome this situation, leading to luminescence of the ion via the "luminescence sensitization" or "antenna effect", defined as a light conversion process involving distinct absorbing (ligand) and emitting (metal ion) components.[37] Moreover, ligand-to-metal charge transfer (LMCT), metal-to-ligand charge transfer (MLCT), and 4f−5d transitions may also canalize energy onto the lanthanide ions.

In this context, attempts were made to record the luminescent spectra in the solid state at room temperature of compounds **1**−**9** exploring several experimental conditions (see section 2 and the Supporting Information). As a result, only compounds **3**, **4** (Type I), and **5** (Type II) show significant emission, and their luminescent features are discussed below.

Upon excitation at 360 nm, compound **3** exhibits orange emission with three characteristic Sm (III) bands at 560, 595, and 640 nm, which are attributed to the radiative decay from the $^4G_{5/2}$ level to the $^5H_{5/2}$, $^6H_{7/2}$, and $^6H_{9/2}$ levels, respectively, as it was observed for other Sm-succinate compounds[10] (see Figure S17, Supporting Information). The corresponding luminescence decay profile is also shown as an inset in Figure S17 (Supporting Information). The experimental curve fits well with single-exponential decay, and a lifetime (τ) of 0.33 ms was determined.

When **4** is excited at 397 nm and **5** at 257 nm, they emit red-orange and green luminescence, respectively. The emission peaks of the compounds correspond to the transitions from $^5D_0 \rightarrow {}^7F_n$ (n = 1−4) at 590, 615, 650, and 700 nm for the Eu(III) ion in **4** (see Figure 10a), and $^5D_4 \rightarrow {}^7F_n$ (n = 6, 5, 4 and 3) transitions at 487, 543, 585, and 619 nm for the Tb(III) ion in **5** (see Figure 11).

The luminescence decay profiles for both compounds are also shown as insets in Figures 10 and 11; they were fitted with single-exponential functions, the resulting τ for **4** and **5** being 0.298 and 1.96 ms, respectively.

The preliminary results presented here suggest that compound **5** exhibits more promising emission features than those of **4**. This fact can be explained in terms of the *concentration quenching of the luminescence*,[38] which seems to be minor for the Tb-framework. The inorganic chains in **5** are separated by 9.1 and 9.4 Å through *trans*-dms conformers, whereas, in the structure of **4**, such chains are separated by 5.9 Å along the *b* direction (via the *gauche*-dms ligands) and 9.5 Å along the *c* direction (via the *trans*-2,3-dms anions). In consequence, in **4** there are planes with higher concentrations of metallic centers that can favor luminescence quenching,

dx.doi.org/10.1021/cg401006d | *Cryst. Growth Des.* 2013, 13, 5249−5260

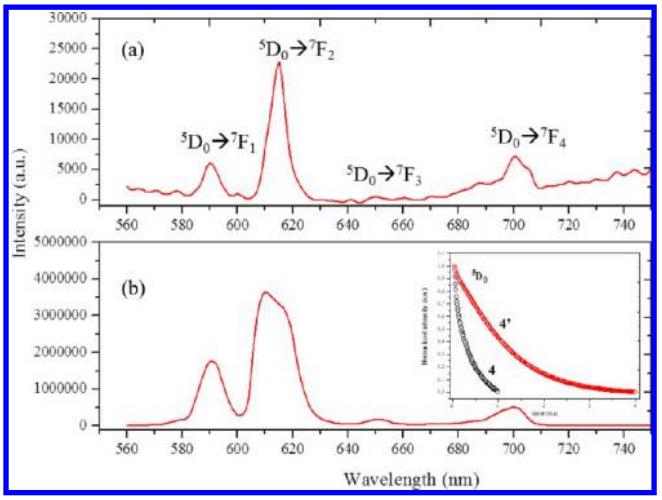

Figure 10. Emission spectra of compounds **4** (a) and **4′** (b). The inset shows the decay curves for both compounds.

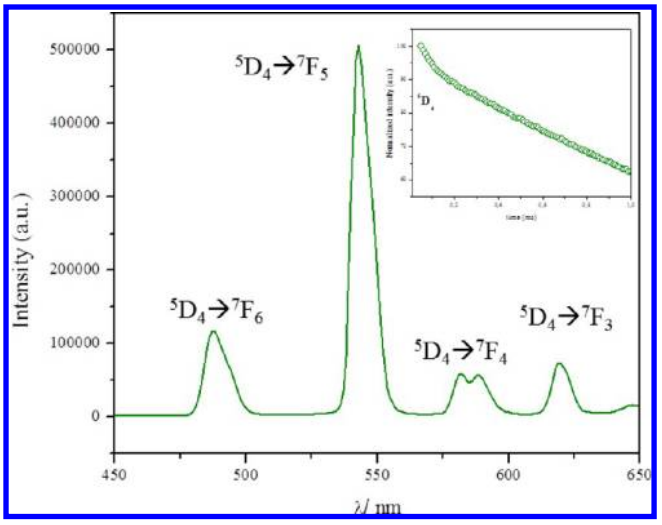

Figure 11. Emission spectrum of compound **5**. The inset shows the decay profile at room temperature.

whereas the wider spacing among chains in **5** prevents or minimizes the occurrence of this effect.

Since the water molecules can quench the luminescence of the lanthanide ions through a nonradiative mechanism involving the vibrational modes of the OH groups, the incidence of dehydration on the PL performance was also investigated. Compound **4** was then selected for this study regarding its strong emission. The emission spectrum of the dehydrated compound **4** (named **4′** from now on) is shown in Figure 10b, from it can be seen that the bands of **4′** are broader than those of **4**, suggesting that the coordination environment in the dehydrated compound is more inhomogeneous than in the latter one.[39] Notably, a red-shifted emission, a marked enhancement of the luminescent intensity, and an increment of the lifetime up to 1.183 ms are observed for **4′** when compares with the emission features of **4**.

However, the best way to compare the PL efficiency of these Eu-MOFs is on the basis of their quantum yields *Q*. For luminescent lanthanide MOFs, the overall luminescence quantum yield is determined by the efficiency of sensitization and by the intrinsic quantum yield (Q_{Ln}) of the lanthanide luminescence. The Q_{Ln} is the quantum yield of the lanthanide-centered luminescence upon direct excitation into the 4f levels, which reflects the extent of nonradiative relaxation processes occurring both in the inner- and in the outer-coordination spheres of the lanthanide ion.[6a] Q_{Ln} can be defined as the simple ratio between the observed and the radiative lifetimes

$$Q_{Ln} = \tau_{obs}/\tau_r \quad (1)$$

where τ_r can be calculated from the following equation

$$1/\tau_r = A_{MD,0} \cdot n^3 \cdot (I_{tot}/I_{MD}) \quad (2)$$

in which $A_{MD,0} = 14.65\ s^{-1}$ is the spontaneous emission probability of the $^5D_0 \rightarrow {}^7F_1$ transition, *n* is the refractive index of the medium (1.5), and the I_{tot}/I_{MD} is the ratio of the integrated total emission from the $^5D_0 \rightarrow {}^7F_J$ transitions (J = 0−6) to the area of the $^5D_0 \rightarrow {}^7F_1$ transition.

The Q_{Ln} for **4** and the dehydrated **4′** were 0.087 and 0.274; these values indicate that compound **4′** emits 3 times more than the water-containing compound **4**, confirming the nonradiative transition processes through OH vibrations of bound water molecules.[40]

To present the nature of the light emitted from the studied compounds, a CIE chromaticity diagram showing their luminescence color is displayed in Figure 12.

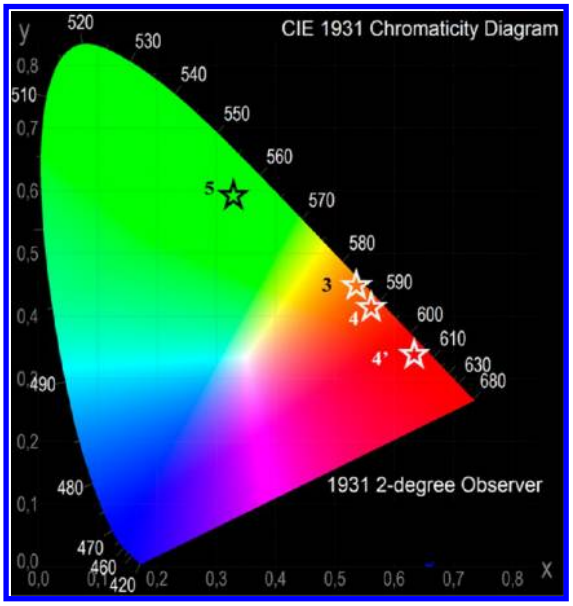

Figure 12. CIE diagram showing the chromaticity coordinates *x,y* for compounds **3** (0.54,0.45), **4** (0.58,0.41), **4′** (0.64,0.35), and **5** (0.33,0.59).

In summary, all peaks in the obtained spectra correspond to transitions within the Ln(III) ion's 4f shell. This suggests that hardly any antenna effect is observed in these compounds. Thus, the luminescence shown by the Ln-MOFs can be obtained by exciting the lanthanide ion directly in its $^{2S+1}L_J$ electronic energy levels, provided that these are at high enough energy to allow the lanthanide-centered luminescence.

4. CONCLUSIONS

Several new Ln(III)-MOFs (Ln = Pr, Nd, Sm, Eu, Tb, Dy, Ho, Er, Yb) based on the 2,3-dimethylsuccinate ligand have been synthesized under the same hydrothermal conditions and characterized by single-crystal and powder X-ray diffraction, IR

spectroscopy, and thermal analysis. All the compounds result in 3D frameworks organized into two different structural types. The compounds involving the "early" Ln(III) ions (Pr–Eu) crystallize in a triclinic structure ($P\bar{1}$ S.G.); their coordination spheres are nine-coordinated and incorporate a water molecule. The MOFs based on the "late" ions (Tb–Yb) are anhydrous and belong to the tetragonal $P4_32_12$ S.G., the metal centers being eight-coordinated. The topological study performed on the novel and the previously reported 3D Ln(III)-dms MOFs allowed us to identify highly symmetric uninodal underlying nets in those cases of frameworks obtained at the highest synthesis temperature and metal content, whereas more complicated simplified nets were obtained when the opposite synthesis conditions are employed. Regarding the first structural type (compounds **1**–**4**), the resulting simplification led to a hexagonal **bnn**-type net, whereas a **fni** topological type was found for the remaining compounds. The PL study allowed the identification of the as-synthesized compounds **3**, **4**, and **5** as orange, red-orange, and green light emitters, the terbium compound being the most promising one. However, the emission spectrum of the dehydrated phase of **4** (**4′**) showed a shift to red and a significant increment in both emission intensity and lifetime, suggesting that, through a dehydration procedure, it is possible to obtain a strong red-emitter material whose emission is 3 times higher than that of the corresponding hydrated compound. These results intend to be a contribution to the development of Ln-MOF materials based on non-conjugated linkers, suitable for the application in photo-luminiscent devices.

■ ASSOCIATED CONTENT

Ⓢ Supporting Information

Crystallographic data in CIF format, synthesis details, powder XRD patterns, Rietveld refinements, TG-DTA curves, and VT-FTIR. This material is available free of charge via the Internet at http://pubs.acs.org.

■ AUTHOR INFORMATION

Corresponding Author

*Fax: 54-266-4430224. E-mail: gnarda@unsl.edu.ar.

Notes

The authors declare no competing financial interest.

■ ACKNOWLEDGMENTS

This work was supported by the Consejo Nacional de Investigaciones Científicas y Técnicas (CONICET: PIP 2008-01360) and Universidad Nacional de San Luis (PROICO 2-1612). G.E.G. acknowledges a Ph.D. CONICET fellowship, G.E.N. and M.C.B. are members of CIC-CONICET. The authors thank Prof. Davide Proserpio and Prof. Michael O'Keeffe for their fruitful comments in the topological analysis of the structures. We would also like to thank Dr. M. Ángeles Monge and Dr. Manuela E. Medina from the Institute of Materials Science of Madrid (ICMM) for XRD single-crystal data collection of compounds **1** and **8**. M.C.B. acknowledges the financial support for the beam time at the BM16 Spanish beam line - ESRF (proposal No. 16-01-741) that allowed obtaining the single-crystal data of compound **3**.

■ REFERENCES

(1) Batten, S. R.; Champness, N. R.; Chen, X.; García Martínez, J.; Kitagawa, S.; Öhrström, L.; Ó Keeffe, M.; Paik Suh, M.; Reedijk, J. *CrystEngComm* **2012**, *14*, 3001–3004.

(2) (a) Murray, L. J.; Dinca, M.; Long, J. R. *Chem. Soc. Rev.* **2009**, *38*, 1294–1314. (b) Hu, Y. H.; Zhang, L. *Adv. Mater.* **2010**, *22*, E117–E130.

(3) (a) An, J.; Geib, S. J.; Rosi, N. L. *J. Am. Chem. Soc.* **2010**, *132*, 38–39. (b) Britt, D.; Furukawa, H.; Wang, B.; Glover, T. G.; Yaghi, O. M. *Proc. Natl. Acad. Sci. U.S.A.* **2009**, *106*, 20637–20640. (c) Wu, H.; Gong, Q.; Olson, D. H.; Li, J. *Chem. Rev.* **2012**, *112*, 836–868. (d) Li, J.-R.; Sculley, J.; Zhou, H.-C. *Chem. Rev.* **2012**, *112*, 869–932. (e) Sumida, K.; Rogow, D. L.; Mason, J. A.; McDonald, T. M.; Bloch, E. D.; Herm, Z. R.; Bae, T.-H.; Long, J. R. *Chem. Rev.* **2012**, *112*, 724–781.

(4) (a) Horcajada, P.; Serre, C.; Maurin, G.; Ramsahye, N. A.; Balas, F.; Vallet-Regí, M.; Sebban, M.; Taulelle, F.; Férey, G. *J. Am. Chem. Soc.* **2008**, *130*, 6774–6780. (b) Della Rocca, J.; Liu, D.; Lin, W. *Acc. Chem. Res.* **2011**, *44*, 957–968. (c) Horcajada, P.; Chalati, T.; Serre, C.; Gillet, V.; Sebrie, C.; Baati, T.; Eubank, J. F.; Heurtaux, D.; Clayette, P.; Kreuz, C.; Chang, J.-S.; Hwang, Y. K.; Marsaud, V.; Bories, P. N.; Cynober, V.; Gil, S.; Férey, G.; Couvreur, P.; Gref, V. *Nat. Mater.* **2010**, *9*, 172–178. (d) Horcajada, P.; Gref, R.; Baati, T.; Allan, P. K.; Maurin, G.; Couvreur, P.; Férey, G.; Morris, R. E.; Serre, C. *Chem. Rev.* **2012**, *112*, 1232–1268.

(5) (a) Czaja, A. U.; Trukhan, N.; Müller, U. *Chem. Soc. Rev.* **2009**, *38*, 1284–1293. (b) Ma, L.; Abney, C.; Lin, W. *Chem. Soc. Rev.* **2009**, *38*, 1248–1256. (c) Corma, A.; García, H.; Llabrés i Xamena, F. X. *Chem. Rev.* **2010**, *110*, 4606–4655. (d) Monge, A.; Gándara, F.; Gutiérrez-Puebla, E.; Snejko, N. *CrystEngComm* **2011**, *13*, 5031–5044.

(6) (a) Bünzli, J.-C. G.; Comby, S.; Chauvin, A.-S.; Vandevyver, C. D. B. *J. Rare Earths* **2007**, *25*, 257–274. (b) Cui, Y.; Yue, Y.; Qian, G.; Chen, B. *Chem. Rev.* **2012**, *122*, 1126–1162. (c) Liu, B. *J. Mater. Chem.* **2012**, *22*, 10094–10101. (d) Niu, D.; Yang, J.; Guo, J.; Kan, W.-Q.; Song, S.-Y.; Du, P.; Ma, J.-F. *Cryst. Growth Des.* **2012**, *12*, 2397–2410. (e) Spencer, E. C.; Zhao, J.; Ross, N. L.; Andrews, M. B.; Surbella, R. G.; Cahill, C. L. *J. Solid State Chem.* **2013**, *202*, 99–104.

(7) (a) Janiak, C. *Dalton Trans.* **2003**, 2781–2804. (b) Krishnan, S. M.; Supkowski, R. M.; LaDuca, R. L. *J. Mol. Struct.* **2008**, *891*, 423–428.

(8) (a) Ghoshal, D.; Kumar Ghosh, A.; Mostafa, G.; Ribas, J.; Ray Chaudhuri, N. *Inorg. Chim. Acta* **2007**, *360*, 1771–1775. (b) Guillou, N.; Livage, C.; Ferey, G. *Eur. J. Inorg. Chem.* **2006**, *24*, 4963–4978. (c) Guillou, N.; Livage, C.; Van Beek, W.; Nogues, M.; Férey, G. *Angew. Chem., Int. Ed.* **2003**, *42*, 644–647. (d) Forster, P. M.; Cheetham, A. K. *Angew. Chem., Int. Ed.* **2002**, *41*, 457–459. (e) Vaidhyanathan, R.; Natarajan, S.; Rao, C. N. R. *Inorg. Chem.* **2002**, *41*, 5226–5234. (f) Burbank, A. R.; O'Sullivan, M. C.; Guillou, N.; Livage, C.; Férey, G.; Stock, N.; Cheetham, A. K. *Solid State Sci.* **2005**, *7*, 1549–1555. (g) Forster, P. M.; Stock, N.; Cheetham, A. K. *Angew. Chem., Int. Ed.* **2005**, *44*, 7608–7611. (h) Forster, P. M.; Burbank, A. R.; Livage, C.; Férey, G.; Cheetham, A. K. *Chem. Commun.* **2004**, *10*, 368–369.

(9) (a) Serpaggi, F.; Férey, G. *Microporous Mesoporous Mater.* **1999**, *32*, 311–318. (b) Seguatni, A.; Fakhfakh, M.; Vauley, M. J.; Jouini, N. *J. Solid State Chem.* **2004**, *177*, 3402–3410. (c) Cui, G.-H.; Li, J.-R.; Zhang, R.-H.; Bu, X.-H. *J. Mol. Struct.* **2005**, *740*, 187–191. (d) Zhang, X. J.; Xing, Y. H.; Han, J. *J. Coord. Chem.* **2008**, *61*, 651–660.

(10) D'Vries, R. F.; Iglesias, M.; Snejko, N.; Alvarez-Garcia, S.; Gutiérrez-Puebla, E.; Monge, M. A. *J. Mater. Chem.* **2012**, *22*, 1191–1198.

(11) Bernini, M. C.; Brusau, E. V.; Narda, G. E.; Echeverria, G. E.; Pozzi, C. G.; Punte, G.; Lehmann, C. W. *Eur. J. Inorg. Chem.* **2007**, 684–693.

(12) Bernini, M. C.; Gándara, F.; Iglesias, M.; Snejko, N.; Gutiérrez-Puebla, E.; Brusau, E. V.; Narda, G. E.; Monge, M. A. *Chem.—Eur. J.* **2009**, *15*, 4896–4905.

(13) Bernini, M. C.; de la Peña-O'Shea, V. A.; Iglesias, M.; Snejko, N.; Gutierrez-Puebla, E.; Brusau, E. V.; Narda, G. E.; Illas, F.; Monge, M. A. *Inorg. Chem.* **2010**, *49*, 5063−5071.
(14) Saines, P. J.; Steinmann, M.; Tan, J. C.; Yeunga, H. H. M.; Cheetham, A. K. *CrystEngComm* **2013**, *15*, 100−110.
(15) Juanhuix, J.; Labrador, A.; Beltran, D.; Herranz, J. F.; Carpentier, P.; Bordas, J. *Rev. Sci. Instrum.* **2005**, *76*, 086103−086104.
(16) Otwinowski, Z.; Minor, W. In *Processing of X-ray Diffraction Data Collected in Oscillation Mode*; Carter, C. W., Jr., Sweet, R. M., Eds.; Methods in Enzymology: Macromolecular Crystallography, Part A; Academic Press: New York, 1997; Vol. *276*, pp 307−326.
(17) *SAINT: Data Collection and Procedure Software for the SMART System*; Siemens Analytical X-ray Instruments, Inc.: Madison, WI, 1995.
(18) *SHELXTL*, version 5.0; Siemens Analytical X-ray Instruments, Inc.: Madison, WI, 1995.
(19) Dowty, E. *ATOMS for Windows 3.1: A Computer Program for Displaying Atomic Structure*; Kingsport, TN, 1995.
(20) Mercury CSD 2.0: New Features for the Visualization and Investigation of Crystal Structures: Macrae, C. F.; Bruno, I. J.; Chisholm, J. A.; Edgington, P. R.; McCabe, P.; Pidcock, E.; Rodriguez-Monge, L.; Taylor, R.; van de Streek, J.; Wood, P. A. *J. Appl. Crystallogr.* **2008**, *41*, 466−470.
(21) Rietveld, H. M. *J. Appl. Crystallogr.* **1969**, *2*, 65−71.
(22) FULLPROF: Rodriguez-Carvajal, J. *Physica B* **1993**, *192*, 55−69.
(23) Cheetham, A. K.; Rao, C. N. R.; Feller, R. K. *Chem. Commun.* **2006**, 4780−4795.
(24) Spek, A. L. *Acta Crystallogr., Sect. A* **1990**, *46*, C34.
(25) Bernini, M. C.; Snejko, N.; Gutierrez-Puebla, E.; Brusau, E. V.; Narda, G. E.; Monge, M. A. *Inorg. Chem.* **2011**, *50/11*, 5958−5968.
(26) Wiberg, K. B. *Acc. Chem. Res.* **1996**, *29*, 229−234.
(27) (a) Brown, K. A.; Martin, D. P.; Supkowski, R. M.; LaDuca, R. L. *CrystEngComm* **2008**, *10*, 846−855. (b) Lyons, E. M.; Braverman, M. A.; Supkowski, R. M.; LaDuca, R. L. *Inorg. Chem. Commun.* **2008**, *11*, 855−858.
(28) (a) Alexandrov, E. V.; Blatov, V. A.; Kochetkov, A. V.; Proserpio, D. M. *CrystEngComm* **2011**, *13*, 3947−3958. (b) ÓKeeffe, M.; Yaghi, O. M. *Chem. Rev.* **2012**, *112*, 675−702.
(29) O'Keeffe, M.; Peskov, M. A.; Ramsden, S. J.; Yaghi, O. M. *Acc. Chem. Res.* **2008**, *41*, 1782−1789. RCSR can be accessed at http://rcsr.anu.edu.au.
(30) Blatov, V. A.; ÓKeeffe, M.; Proserpio, D. M. *CrystEngComm.* **2009**, *12*, 44−48.
(31) (a) Blatov, V. A. *IUCr Computing Commission Newsletter*; IUCr: Chester, U.K., **2006**; No. 7, pp 4−38. (b) Blatov, V. A.; Carlucci, L.; Ciani, G.; Proserpio, D. M. *CrystEngComm* **2004**, *6*, 377−395.
(32) Delgado-Friedrichs, O.; O'Keeffe, M. *Acta Crystallogr.* **2003**, *A59*, 351−360.
(33) Rosi, N. L.; Kim, J.; Eddaoudi, M.; Chen, B.; O'Keeffe, M.; Yaghi, O. M. *J. Am. Chem. Soc.* **2005**, *127*, 1504−1518.
(34) Bernini, M. C.; Brusau, E. V.; Narda, G. E.; Echeverria, G.; Fantoni, A.; Punte, G.; Ayala, A. P. *Polyhedron* **2012**, *1*, 729−737.
(35) (a) Maspoch, D.; Ruiz-Molina, D.; Veciana, J. *Chem. Soc. Rev.* **2007**, *36*, 770−818. (b) Suh, M. P.; Cheon, Y. E.; Lee, E. Y. *Coord. Chem. Rev.* **2008**, *252*, 1007−1026. (c) Luo, F.; Batten, S. R. *Dalton Trans.* **2010**, *39*, 4485−4488.
(36) (a) Allendorf, M. D.; Bauer, C. A.; Bhakta, R. K.; Houk, R. J. T. *Chem. Soc. Rev.* **2009**, *38*, 1330−1352. (b) Decadt, R.; Van Hecke, K.; Depla, D.; Leus, K.; Weinberger, D.; Van Driessche, I.; Van Der Voort, P.; Van Deun, R. *Inorg. Chem.* **2012**, *51*, 11623−11634. (c) Chaudhari, A. K.; Nagarkar, S. S.; Joarder, B.; Ghosh, S. K. *Cryst. Growth Des.* **2013**, *13*, 3716−3721. (d) D'Vries, R. F.; Alvarez-García, S.; Snejko, N.; Bausá, L. E.; Gutiérrez-Puebla, E.; de Andrés, A.; Monge, M. A. *J. Mater. Chem. C* **2013**, *1*, 6316−6324.
(37) Sabbatini, N.; Guardigli, M.; Manet, I.; Ungaro, R.; Casnati, A.; Ziessel, R.; Ulrich, G.; Asfari, Z.; Lehn, J. M. *Pure Appl. Chem.* **1995**, *67*, 135−140.
(38) Gándara, F.; de Andrés, A.; Gómez-Lor, B.; Gutiérrez-Puebla, E.; Iglesias, M.; Monge, M. A.; Proserpio, D. M.; Snejko, N. *Cryst. Growth. Des.* **2008**, *8*, 378−380.
(39) Kim, Y.; Suh, M.; Jung, D.-Y. *Inorg. Chem.* **2004**, *43*, 245−250.
(40) (a) Binnemans, K. Rare Earth *β*-Diketonate Complexes: Functionalities and Applications. In *Handbook on the Physics and Chemistry of Rare Earths*; Gschneidner, K. A., Jr., Bünzli, J. C. G., Pecharsky, V. K., Eds.; Elsevier Science B.V.: Amsterdam, 2005; Vol. *35*, Chapter 225, p 173. (b) Binnemans, K. *Chem. Rev.* **2009**, *109*, 4283−4374.